Pergamon

Canadian Metallurgical Quarterly, Vol. 38, No. 5, pp. 363–375, 1999

0008-4433/00 $20.00 + 0.00

PII: S0008-4433(99)00028-2

MEASUREMENT AND MODELING OF HEAT TRANSFER ACROSS INTERFACIAL MOLD FLUX LAYERS

DAVID T. STONE† and BRIAN G. THOMAS‡*

†The Boeing Company, 5301 Bolsa Avenue, MC H011-C132, Huntington Beach, CA 92647, USA and ‡Department of Mechanical and Industrial Engineering, University of Illinois, Urbana-Champaign, 1206 West Green Street, Urbana, IL 61801, USA

(*Received* 1 *October* 1999; *in revised form* 1 *October* 1999; *accepted* 1 *October* 1999)

Abstract—Surface quality problems in continuous cast steel are greatly affected by heat transfer across the interfacial layers in the gap between the solidifying steel shell and the mold. An experimental apparatus has been constructed to measure temperatures in the steel, mold flux layers, and copper under conditions approximating those in continuous casting. The flux solidified in multiple layers similar to those observed from continuous casting molds and contained many gas bubbles. Flux conductivities average about 1.0 W/m·K and appear to evolve with time. Contact resistances at both interfaces are significant and average about 0.0015 $m^2 \cdot K/W$. Flux crystallization appears to be the only significant effect of flux composition. The one glassy flux tested had much greater thermal conductivities, presumably due to radiation transport. Temperature and gap thickness had a negligible effect on the properties. These properties depend on the model used to extract them. They are being implemented into a mathematical model to simulate heat transfer in the mold, interface, and solidifying shell of a continuous slab-casting machine. © 2000 Canadian Institute of Mining and Metallurgy. Published by Elsevier Science Ltd. All rights reserved.

Résumé—Les problèmes de qualité de surface de l'acier de coulée continue sont grandement affectés par le transfert de chaleur à travers les couches interfaciales dans l'intervalle entre la gaine d'acier en train de se solidifier et le moule. On a construit un appareil expérimental afin de mesurer la température de l'acier, des couches d'écoulement du moule et du cuivre sous des conditions approchant celles de la coulée continue. L'écoulement s'est solidifié en couches multiples similaires à celles observées dans les moules de coulée continue et celles-ci contenaient plusieurs bulles de gaz. La moyenne de conductivité de l'écoulement est d'environ 1.0 W/m·K et semble évoluer avec le temps. La résistance de contact aux deux interfaces est importante et atteint en moyenne environ 0.0015 $m^2 \cdot K/W$. La cristallisation de l'écoulement paraît être le seul effet important de la composition du flux. Le seul écoulement vitreux évalué avait une conductivité thermique beaucoup plus élevée, vraisemblablement dû au transport par radiation. La température et la largeur de l'intervalle avaient un effet négligeable sur les propriétés. Ces propriétés dépendent du modèle utilisé pour les extraire. On est en train de les développer en un modèle mathématique afin de simuler le transfert de chaleur dans le moule, à l'interface et dans la gaine de solidification d'un appareil de coulée continue de brame. © 2000 Canadian Institute of Mining and Metallurgy. Published by Elsevier Science Ltd. All rights reserved.

NOMENCLATURE

a	flux absorption coefficient (m^{-1})
d	distance (m)
d_{osc}	effective mark thickness (volume)
d_s, d_l	thickness of solid, liquid flux layers (m)
d_{oeff}	effective oscillation mark depth (mm) (thermal)
d_{mark}	maximum oscillation mark depth (mm)
k	thermal conductivity (W m^{-1} K^{-1})
K_{mark}	oscillation mark conductivity (W m^{-1} K^{-1})
K_f	conductivity of rest of gap (W m^{-1} K^{-1})
L_{mark}	width of oscillation marks (mm)
L_{pitch}	ratio of casting speed to oscillation frequency (mm)
m	flux refractive index
$\dot{q}$	heat flux (W/m^2)
Q_f	mold flux consumption (kg m^{-2})
R	interface resistance (m^2 K W^{-1})
T	temperature (K)
T_{Cu}	mold surface temperature (°C)
T_{Fe}	steel surface temperature (°C)
V_c	casting speed (m s^{-1})
V_l	liquid flux velocity (m s^{-1})
V_s	solid flux velocity (m s^{-1})

Greek symbols

σ	Stefan–Boltzmann constant (W m^{-2} K^{-4})
ρ_{flux}	flux density (kg m^{-3})
ϵ_{Fe}, ϵ_{Cu}	steel, mold surface emissivities

*Author to whom correspondence should be addressed. Tel.: +1-217-333-6919; fax: +1-217-244-6534. E-mail: bgthomas@uiuc.edu.

Subscripts
1 thermocouple set 1
2 thermocouple set 2
C copper thermocouple near cold face
Cu copper
Fe steel
flux flux
G gap
gap pertaining to gap
H copper thermocouple near hot face
I interface

INTRODUCTION

Over 80% of the steel produced in North America is continuously cast. Figure 1 shows a schematic of the process that includes the critical meniscus region in the mold, where the majority of quality defects originate. The surface of the final product is created during the initial stage of solidification of the steel shell against the water-cooled copper mold at the meniscus. Turbulence at the top surface, level fluctuations, freezing of the meniscus and the generation or entrainment of inclusions are all potential causes of quality problems. Many of these problems can be reduced with the use of an optimal mold flux, which is depicted in Fig. 1.

Mold flux is added as a powder to the top surface, where it insulates the molten steel from both heat loss and contamination by the atmosphere. The powder sinters and melts to form a layer of liquid that floats on the surface of the molten steel. The liquid flux then infiltrates into the gap between the solidifying steel shell and the mold walls. Here it acts as a lubricant to prevent sticking of the shell to the mold. It also controls the rate of heat conduction across the interfacial gap that in turn governs heat removal from the shell. Mold flux operations require pouring the steel from the tundish through a submerged entry nozzle. This has the added benefit of further protecting the steel from the atmosphere and controlling the flow pattern in the mold.

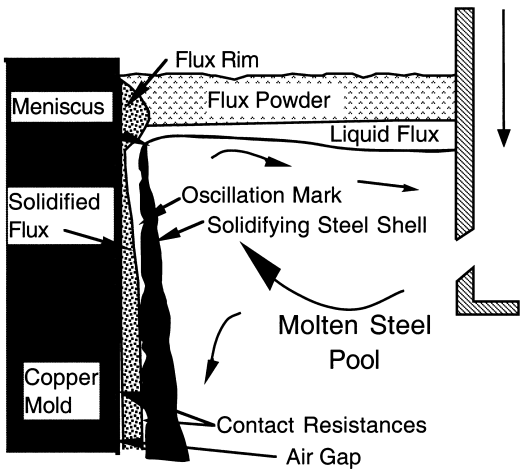

Fig. 1. Schematic of continuous casting process showing casting flux layers.

This type of operation is typical of all continuous slab and bloom casters. Mold flux is also finding increasing use in billet casting, particularly when a high quality product is required. It may also offer advantages when casting billets at high speed.

One of the critical functions of the mold flux is to control heat transfer across the interfacial gap. Liquid mold flux enters this gap at the meniscus intermittently during each oscillation cycle. It solidifies in the cold side of the gap into layers which may contain either crystalline or glassy phases, depending on the composition and local cooling history [1, 2]. These flux layers govern heat transfer across the gap.

Heat transfer across the interfacial gap greatly affects steel quality. For example, the lower heat transfer rate near the meniscus associated with high-solidification-temperature mold fluxes improves the surface quality of crack-sensitive peritectic (0.1–0.2°C) steel grades [3] and reduces longitudinal cracks [4]. The uniformity of this initial heat transfer rate, as well as its magnitude, is very important [5, 6]. Non-uniform heat transfer generates thermal stresses in the shell, which are worsened by differences in thermal contraction of δ austenite and γ ferrite. This produces non-uniform shell growth, which leads to a variety of quality problems including deep oscillation marks (and subsequent transverse cracks), localized hot, weak regions which concentrate strain and form longitudinal cracks, and surface shape problems such as rhomboidity [7]. In the extreme, breakouts may occur when the taper of the mold walls does not match the shell shrinkage. Insufficient taper (related to unexpectedly high heat transfer) might cause an air gap, where regions of the shell become too weak to support the liquid pool below the mold. Excessive taper (related to unexpectedly low heat transfer) may cause jamming of the shell in the mold. These problems are best avoided by understanding and controlling heat transfer across the interfacial gap.

The rate of heat transfer across the interfacial gap depends mainly on the properties of the mold flux filling the gap. These properties include phonon and photon conductivity [8], radiative properties such as emissivity and absorption coefficient [9], and contact resistances, especially where the flux is solid. This paper focuses on the application of laboratory experiments and mathematical models to improve understanding of heat transfer across mold flux layers.

PREVIOUS WORK

Several researchers have performed experiments to measure the thermal properties of mold fluxes under thermal conditions designed to simulate those in the gap during continuous casting of steel. The measured properties depend greatly on the model used to derive those properties, so experiments and models must be discussed together.

Ohmiya [10] simulated the mold/strand gap by lowering a cooled copper block into a layer of molten mold flux that was resting on a steel plate heated by an electric current. Heat transfer through the powder was measured by three thermocouples (two in the copper mold and one in the steel).

Data was obtained for several test materials (with known conductivities) and three commercial mold powders. Effective thermal conductivity, k_{gap}, quantifies heat transfer across the entire gap width, d_{gap}, from all mechanisms combined together, including standard (phonon) conduction, radiation (photon) conduction, and the effect of contact resistances:

$$\dot{q} = k_{gap}\frac{T_{Fe} - T_{Cu}}{d_{gap}} \tag{1}$$

where T_{Fe} and T_{Cu} are the surface temperatures of the hot steel and cold copper that face the gap. In addition to reporting the raw data and gap conductivities, thermal properties can be obtained by fitting the data to an equation that includes both conduction and radiation terms (acting independently):

$$\dot{q} = \gamma_1(T_{Fe} - T_{Cu}) + \gamma_2(T_{Fe}^4 - T_{Cu}^4) \quad \text{where} \quad \gamma_1 = \frac{k_{flux}}{d_{gap}}$$
$$\text{and} \quad \gamma_2 = \frac{m^2\sigma}{0.75ad_{gap} + 1/\epsilon_{Fe} + 1/\epsilon_{Cu} - 1} \tag{2}$$

Values of mold flux thermal conductivity, k_{flux}, calculated in this way ranged between 0.22 and 0.43 W/m·K. The radiation component was significant. Furthermore, the fitted parameters were still strong functions of the thickness of the flux layer, indicating that these thermal properties are not fundamental. This is likely due to the temperature dependence of the properties, especially the absorption coefficient, a, which is reported to be a strong function of wavelength and increases if crystallization occurs [5, 9]. The error (underprediction of heat flux) due to ignoring the interaction between the conduction and radiation terms is predicted to be less than 6% [11].

Mills and coworkers have conducted many experimental measurements of mold flux properties [5, 9, 12]. The thermal conductivity of mold powders and solidified mold flux films were extracted using the laser pulse method. In this method, a laser pulse is directed onto the front face of the specimen and the temperature transient of the rear face is recorded continuously. Thermal conductivity is derived by estimating the thermal diffusivity and taking the density, ρ, and specific heat, C_p, from previous measurements:

$$k_{gap} = \rho C_p \frac{0.1388 d_{gap}^2}{t_{0.5}} \tag{3}$$

Here, $t_{0.5}$ is the time taken to reach half of the maximum temperature rise. Molten flux conductivities of 1.3 to 2.5 W/m·K were reported, with values of glassy films being much lower than those of partially crystalline films. This conductivity is an effective value, which includes both conduction and radiation components. After extensive investigation, Mills concluded that variations in heat transfer between different trials were not caused by any composition dependence of the flux conductivity.

The absorption coefficient of glassy films can be predicted by the empirical relation [13] $a\ (m^{-1}) = 910 \cdot (\%FeO)$. For crystalline slags, absorption is much greater, with reported extinction coefficients of 100,000 m^{-1} [9]. Even in predominantly glassy films, where radiation conduction is more important, its contribution to the total heat flux [the second term in eqn (2)] was predicted to be less than 10% under continuous casting conditions [5]. Total normal emissivities of around 0.9 were measured.

Mikrovas [14] utilized the "copper finger" method to measure the thermal properties of thick slag layers. In this method, a chilled copper cylinder is immersed in a bath of molten flux, and temperatures measured within the flux and copper. A transient model was used to extract the effective conductivity [eqn (1)]. Conductivities of 1.2 to 1.5 W/m·K were measured near the melting temperature, while values up to 4.0 W/m·K were obtained when the slag was superheated by 400°C. The increase was attributed to the greater importance of radiation at the higher temperatures and in thicker flux layers. Mikrovas also observed a drop in conductivity with increasing TiO_2 content. Finally, additional experiments and calculations estimated the interfacial resistance between the copper cylinder and the mold flux layer to be 8.8×10^{-4} $m^2 \cdot K/W$, together with an effective conductivity of 3.0 W/m·K.

Jenkins [1], using a more sophisticated copper finger apparatus, obtained values of thermal conductivity of around 1.0 W/m K, and absorption coefficients of around 350 m^{-1}. Contact resistances of $1–3 \times 10^{-4}$ $m^2 \cdot K/W$ were measured. Jenkins also investigated the effect that doping mold powders with transition metal oxides had on radiative heat transfer across the mold/strand gap.

Susa [13] utilized the hot strip method to measure thermal conductivity, thermal diffusivity, and specific heat of mold powders containing iron oxides. Many different chemical compositions of mold powders were tested, and values of thermal conductivity were measured to be between 1.5 and 2.2 W/m·K at temperatures below 1200 K. Above 1200 K, conductivity values decreased with increasing temperature, which is possibly due to the increased dominance of radiation in total mold heat transfer. Mold flux specific heat increases with increasing temperature, especially above the glass transition temperature.

Yamauchi [15] simulated the mold/strand gap by heating previously solidified mold flux samples between a heated AlN plate and a cooled block of 304 stainless steel. Four different powders were tested, and data was evaluated with a 1-D heat transfer model:

$$\dot{q} = \frac{T_{Fe} - T_{Cu}}{d_{gap}/k_{eff} + R_{int}} \tag{4}$$

Most of the test conditions were well below the flux solidification temperatures, and conductivities of 0.6 to 1.3 W/m·K were reported. Further investigation into the radiative component of the heat transfer revealed that the radiation conductivity was approximately 20% of the total heat transfer. Interfacial air gaps of between 0.004–0.008 $m^2 \cdot K/W$ were observed for solid fluxes. Negligible resistances were measured above the flux melting temperature. Also, k_{eff} was observed to decrease with increasing mold powder basicity (CaO/SiO_2).

This section has illustrated the variety of previous experiments and models that have been used to quantify the thermal properties of mold fluxes. The present work aims to measure mold flux properties under conditions that match the thermal histories experienced by the liquid flux in the continuous casting process. In addition, extra thermocouples will be used in the interfacial gap, in order to distinguish the contributions of the flux conductivity and interface resistances. Any changes in the properties with time will be observed.

EXPERIMENTS

Apparatus description

An apparatus was constructed to simulate the conditions experienced by the liquid mold flux in the gap near the meniscus in the continuous casting process. Figure 2 shows the apparatus, which includes a machined block of 9.99% pure copper to represent the mold, and a 3.17-mm thick plate of 409 stainless-steel hot band to represent the surface of the solidifying steel shell. The thickness of the gap was controlled by inserting stainless steel spacers of known thickness between the steel plate and copper block prior to bolting them together. To minimize contact between the hot steel and cold copper, one of the spacers with a thin (1.0-mm diameter) stainless steel wire. Heat was provided to the outside of the steel plate by an oxyacetylene torch. Its position was adjusted to control the steel temperature. The copper mold was cooled by flowing 25°C water at 0.08–0.11 l/s through 9.525 mm (3/8″) diameter copper tubing, which was bent into a flat coil and squeezed against the back of the copper mold using bolts.

The design of the copper mold and thermocouple placement are shown in Figs 3 and 4. The steel hot band was connected to the copper mold by seven steel bolts. Seven thermocouples were used to measure temperatures within the apparatus. Steel surface temperature, T_{Fe}, was measured with a type-S thermocouple spot-welded to the gap side of the steel plate. Two type-K thermocouples were placed at predefined depths within the flux gap to measure flux film temperatures, T_{G1} and T_{G2}. Two pairs of type-K thermocouples were silver-soldered into the copper mold to measure mold temperatures (T_{H1} and T_{C1}, T_{H2} and T_{C2}) and to calculate two sets of heat fluxes. Note that set 1 is near the center of the heat input, while set 2 is lower down. The thermocouples were connected through an A/D serial board, to a laptop data acquisition system. Temperatures were recorded from each thermocouple every 3 s (0.33 Hz). The assembled apparatus was surrounded by refractory brick, zirconium paper, and Kao-wool to reduce heat losses.

Mold flux preparation

Mold powder samples were decarburized at 1100°C for about 8 h prior to each experiment. The powder was then melted in a graphite crucible inside an induction furnace. Argon was introduced through a layer of alumina insulation placed between the crucible and the furnace in order to protect the crucible from oxidation. Once the liquid flux reached about 200°C above its crystallization temperature, a sample of molten flux was scooped up with a steel spoon

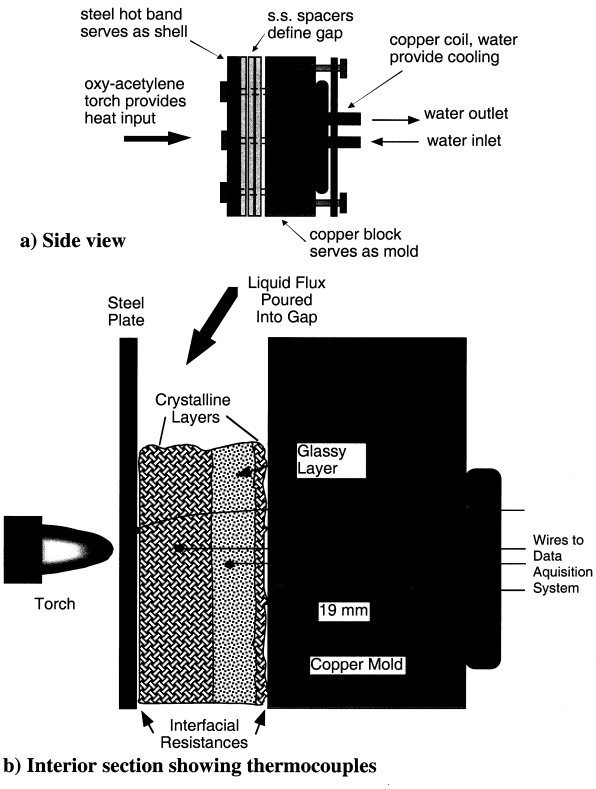

Fig. 2. Schematic of experimental apparatus. (a) Side view. (b) Interior section showing thermocouples.

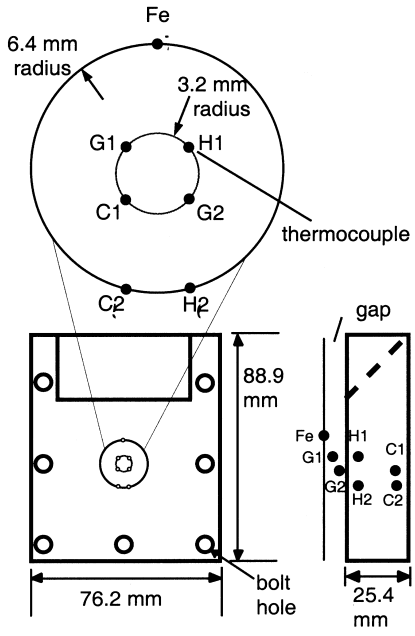

Fig. 3. Copper mold design and thermocouple placement.

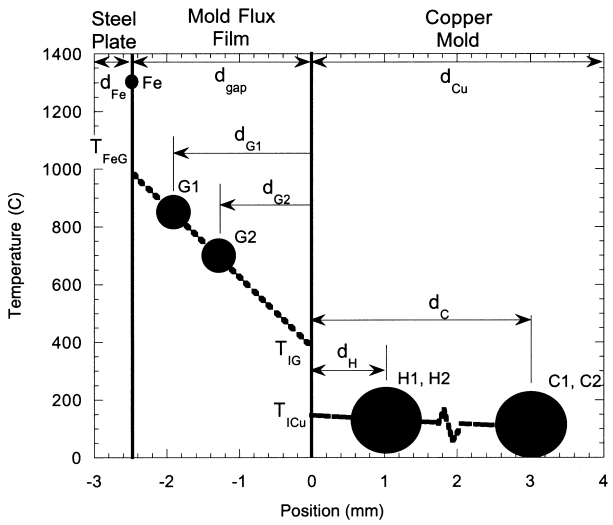

Fig. 4. Typical temperature distribution measured in apparatus showing size of thermocouples.

and poured into the top of the mold apparatus. The composition of each of the four mold fluxes tested is given in Table 1, along with other properties provided by the manufacturers.

Experimental procedure

First, the mold apparatus is preheated with the torch until the steel temperature reaches about 1300°C and the data acquisition system is started. Then, the liquid flux is poured into the apparatus, the cooling system is turned on, and the top covered with Kao-wool. The torch position is adjusted to maintain the steel temperature at about 1300°C. Data is recorded for about 1–2 min. The torch is then moved to carefully lower the steel temperature in 100°C increments to 900°C. The temperature is maintained at each increment in order for steady state to develop. To investigate reproducibility and the importance of time in the apparatus, the steel temperature was increased to 1300°C again and the step cooling sequence repeated. After the system had cooled to ambient, the apparatus was carefully taken apart and the final position of the gap thermocouples, flux layer thickness, and plate shape was measured. Finally, micrographs of the flux microstructures were taken.

Table 1. Compositions (mass percent) and other properties of tested mold powders

	Flux A	Flux B2	Flux C	Flux D
SiO_2	33.80	29.93	38.40	40.80
CaO	33.90	39.41	39.20	36.70
Al_2O_3	6.20	4.58	5.00	5.60
MgO	2.40	0.79	3.40	3.40
Na_2O	10.60	9.04	2.00	2.16
F	5.70	12.93	9.30	7.20
Total carbon	4.10	2.18	2.60	
CaO/SiO_2	1.00	1.32	1.02	0.90
Viscosity at 1300°C (poise)	2.30	0.30	2.00	4.00
Crystallization temperature (°C)	1146	1180	1135	1110

Table 2 summarizes the conditions of the 16 experiments performed, which include three different initial gap sizes (1.5, 2.5, and 3.5 mm) for the four different mold fluxes. Several experiments are replicated to evaluate the reproducibility.

Data analysis

The idealized temperature profile, through the experimental apparatus during a typical test, is shown in Fig. 4. This figure defines the thermocouple temperatures and distances used in the following equations. It also illustrates the large size of the thermocouples relative to the gap dimensions. This is one source of uncertainty in the interpretation of the measurements, especially those in the gap.

The total heat flux was derived from each pair of thermocouples in the copper mold. Calculations using a 2-D model revealed that 2-D effects were negligible, so the following 1-D equation could be employed with reasonable accuracy:

$$\dot{q} = k_{\mathrm{Cu}} \frac{(T_{\mathrm{H1}} - T_{\mathrm{C1}})}{d_{\mathrm{C}} - d_{\mathrm{H}}} \quad \text{or } k_{\mathrm{Cu}} \frac{(T_{\mathrm{H2}} - T_{\mathrm{C2}})}{d_{\mathrm{C}} - d_{\mathrm{H}}} \tag{5}$$

Copper conductivity, k_{Cu}, was assumed to be 388·W/m K. In the calculations that follow, different values are obtained depending on whether heat flux is calculated using mold thermocouples from set 1 or 2. These can be compared to illustrate the variability. Effective conductivity across the gap is derived from the heat flux via:

$$k_{\mathrm{gap}} = \frac{\dot{q}\, d_{\mathrm{gap}}}{T_{\mathrm{Fe}} - T_{\mathrm{ICu}}} \quad \text{where} \quad T_{\mathrm{ICu}} = T_{\mathrm{H}} + \frac{\dot{q}\, d_{\mathrm{H}}}{k_{\mathrm{Cu}}} \tag{6}$$

The final gap thickness, d_{gap}, is included in Table 2, as the

Table 2. Experimental conditions

Experiment	Mold flux	Initial gap (mm)	Thermocouple locations (distance from mold hot face-mm)*						
			Fe	G1	G2	H1	C1	H2	C2
1	A	2.5	2.00	0.75	−1.0	−3.0	−1.0	−3.0	
2		3.5	3.00	1.50	−1.0	−3.0	−1.0	−3.0	
3		3.5	3.00	1.50	−1.0	−3.0	−1.0	−3.0	
4	B2	2.5	3.0	2.00	1.00	−1.0	−20.0	−1.0	−20.0
5		2.5	2.8	2.54	1.32	−1.0	−20.0	−1.0	−20.0
6		3.5	3.00	1.50	−1.0	−20.0	−1.0	−20.0	
7		3.5	2.82	1.64	−1.0	−20.0	−1.0	−20.0	
8	C	2.5	2.7	1.92	1.23	−1.0	−20.0	−1.0	−20.0
9		2.5	3.1	2.39	1.02	−1.0	−20.0	−1.0	−20.0
10		3.5	3.00	1.55	−1.0	−20.0	−1.0	−20.0	
11	D	1.5	1.7	1.23	0.51	−1.0	−20.0	−1.0	−20.0
12		1.5	1.00	0.50	−1.0	−20.0	−1.0	−20.0	
13		2.5	2.00	1.00	−1.0	−20.0	−1.0	−20.0	
14		2.5	2.00	1.00	−1.0	−20.0	−1.0	−20.0	
15		3.5	3.8	3.11	1.97	−1.0	−20.0	−1.0	−20.0
16		3.5	4.0	3.20	1.50	−1.0	−20.0	−1.0	−20.0

* Negative numbers reference distances towards back of mold.

final location of the Fe thermocouple. Next, the gap thermocouples were used to isolate the relative contributions of radiation/conduction and contact resistance on the effective gap conductivity. Specifically, flux conductivity was estimated by:

$$k_{\text{flux}} = \frac{\dot{q}(d_{\text{G1}} - d_{\text{G2}})}{T_{\text{G1}} - T_{\text{G2}}} \tag{7}$$

The flux/mold contact resistance was then estimated by:

$$R_{\text{Cu}} = \frac{(T_{\text{IG}} - T_{\text{ICu}})}{\dot{q}} \quad \text{where} \quad T_{\text{IG}} = T_{\text{G2}} - \frac{\dot{q}\, d_{\text{G2}}}{k_{\text{flux}}} \tag{8}$$

The flux/steel contact resistance was estimated by:

$$R_{\text{Fe}} = \frac{(T_{\text{Fe}} - T_{\text{FeG}})}{\dot{q}} \quad \text{where} \quad T_{\text{FeG}} = T_{\text{G1}} + \frac{\dot{q}(d_{\text{gap}} - d_{\text{G1}})}{k_{\text{flux}}} \tag{9}$$

TRANSIENT RESULTS

The temperature histories of all seven thermocouples are given in Fig. 5 for a typical experiment, No. 8. The extracted histories of heat flux, thermal conductivity and interface resistances are given in Figs 6–8.

Initial transient

A striking feature, observed in all experiments, is a sharp spike in the temperature of all thermocouples in the first few seconds after pouring the liquid flux into the mold. An apparent spike in the heat flux and gap conductivity accompanies this phenomenon, as shown in Figs 6 and 7.

Calculations using a simple transient model predict that the thin layer of mold flux should solidify against the chilled copper in 1–5 s, depending on the gap thickness. During this brief initial time, heat is supplied to the mold by the heat content of the molten flux and not by a high rate of conduction. The recorded peaks in both the gap thermocouples and mold surface temperatures are consistent with these calculations. A similar effect is likely to occur at the meniscus in an operating caster. Steady state is reached after only a few seconds, so this transient effect does not explain the persistence of high temperatures, and correspondingly high heat fluxes, that are observed after longer times in some experiments.

Just after pouring in the flux, the steel surface temperature dips slightly, which causes a corresponding drop in all of the temperatures. This is due to the delay in increasing heat input from the torch to maintain the greatly increased heat transfer across the now-highly conductive gap. This is a second reason for the sharp initial drop in heat flux.

Error analysis

Differences between heat fluxes calculated using the two sets of mold thermocouples were always observed, with set 1 being consistently lower. Experiment 8 is a particularly extreme example, as Fig. 6 shows differences of up to 30%. This may be due to slight differences in the gap thickness at these two locations.

The set 1 thermocouples were closer to the center of the mold (see Fig. 3). where the flux layer was thicker due to outward distortion of the steel plate. Figure 9 compares the initial and final flux layer thicknesses and plate dimensions for different locations and experiments. This figure shows that the final flux layer is always about 10% thicker near the center. Figure 9 also confirms that the plate expands the most in the center. It is likely that this expansion away from the flux film generates a slightly larger air gap at the center, which also contributes to the set 1 values being lower. Only the final dimensions could be measured, but the evolution of the plate shape during the experiment is likely responsible for most of the differences between the two thermocouple sets.

Thermal conductivity

An example of the calculated thermal conductivity histories is shown in Fig. 7, based on thermocouple set 1. Results for set 2 are very similar. The effective gap conductivity is surprisingly insensitive to variation during the experiment (after the initial transient, which is an artifact as

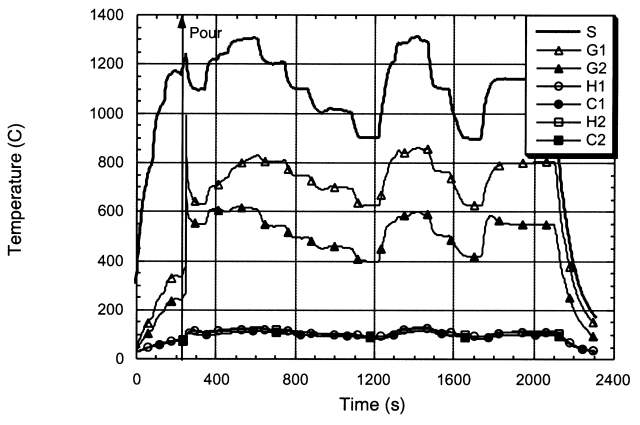

Fig. 5. Typical temperature histories measured by each thermocouple (experiment 8).

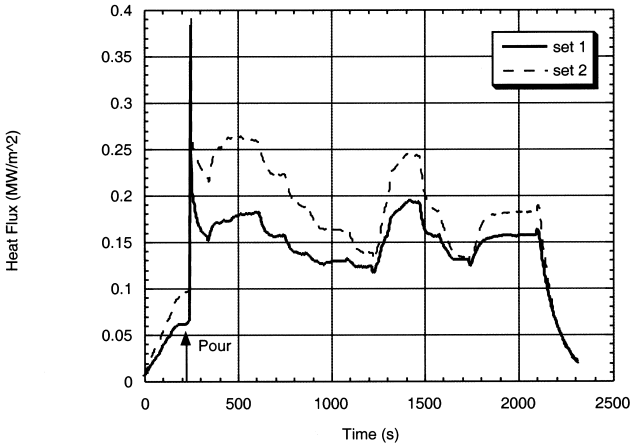

Fig. 6. Heat flux [based on eqn (5) for experiment 8].

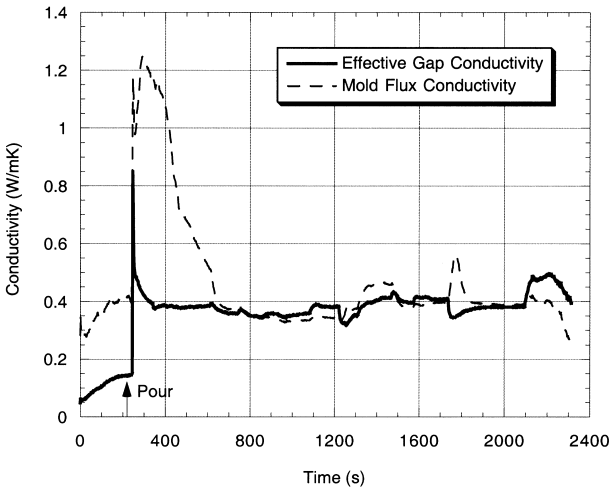

Fig. 7. Conductivity (experiment 8, mold thermocouple set 1).

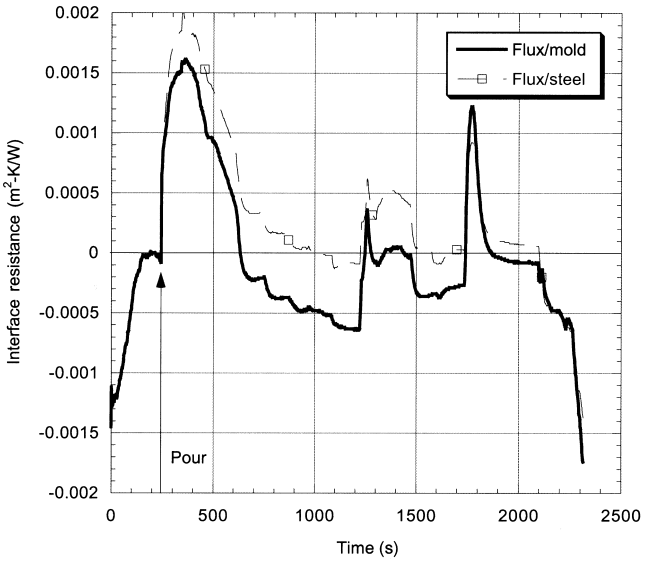

Fig. 8. Interface resistances (experiment 8, mold thermocouple set 1).

explained above). The flux conductivity based on the gap thermocouples, however, remained very high for nearly 400 s after pouring. This was offset by a corresponding high initial value of the contact resistance, which is shown in Fig. 9. The conductivity dropped from 1.2 to 0.4 W/m·K, where it remained virtually constant for the rest of the experiment, despite the many temperature changes imposed.

This dramatic change in conductivity with time was rarely as dramatic as in this experiment, so it is possible that a simple error, such as a shift in the position of one of the gap thermocouples, was responsible. The relatively large size of the gap thermocouples, shown in Fig. 4, suggests that slight changes in their locations could greatly influence the flux conductivity and contact resistance results. However, slight drops in flux conductivity were often observed within several minutes after pour. Minor changes in conductivity with time were always observed. Figure 10 shows the evolution of gap conductivity with both time and temperature for experiment 8. The minor variations observed do not appear to correspond with temperature changes.

If the effect of time on mold flux thermal properties is real, it may correspond to a change in microstructure, such as caused by crystallization. The time-dependent nature of these changes has recently been confirmed [2] and is being quantified in controlled laboratory experiments designed to characterize the nucleation kinetics as Time-Temperature-Transformation diagrams for mold fluxes. After becoming crystalline, the flux conductivity is expected to drop, so this observation seems plausible.

Interface resistance

Figure 8 shows the evolution of the interface resistances with time for this example (experiment 8, set 1). Both the flux/mold and flux/steel interfaces behave in a surprisingly similar manner. Note that each time the temperature is increased (at 1250 and 1750 s), the interface resistances jump sharply. This behavior was observed in most experiments whenever subsequent reheating occurred. It is believed to be due to reheating causing the steel plate to warp away from the solid mold flux layer, which creates an additional air gap. An air gap of 0.1 mm (100 μm) corresponds to an interface resistance of 0.0017 $m^2 \cdot K/W$, so this explanation seems feasible.

The apparatus in this work maintains a rigid gap that does not squeeze the solidifying flux against the copper and steel plates. Thus, thermal contraction of the solidifying mold flux is able to generate a contact resistance. This is the opposite of experiments that use a copper finger, where thermal contraction of the mold flux around the finger decreases contact resistance. Thus, it is expected that the contact resistances observed in this work should be larger than the values of 1–9 $\times$ 10^{-4} $m^2 \cdot K/W$ observed in copper finger experiments. It is believed that the conditions of the present experiment likely hold in the continuous casting mold, especially near the corners and further below the meniscus, where the steel shell is strong enough to maintain a rigid gap.

Mold flux microstructure

Figures 11 and 12 show the final microstructures of sections of the gap taken through typical solidified flux samples. The particular fluxes illustrated, C and D, exhibit a complex multiple layered structure that is similar in appearance to flux samples removed from operating continuous casting molds. More different layers can be distinguished by their unique colors than is obvious in these two figures. Most of the layers appear mainly crystalline, which could explain the apparent lack of sensitivity of the conductivities to temperature. This is consistent with the findings of Mills that radiation makes less than a 10% difference to the heat transfer. Only samples taken of flux A revealed a fully glassy structure.

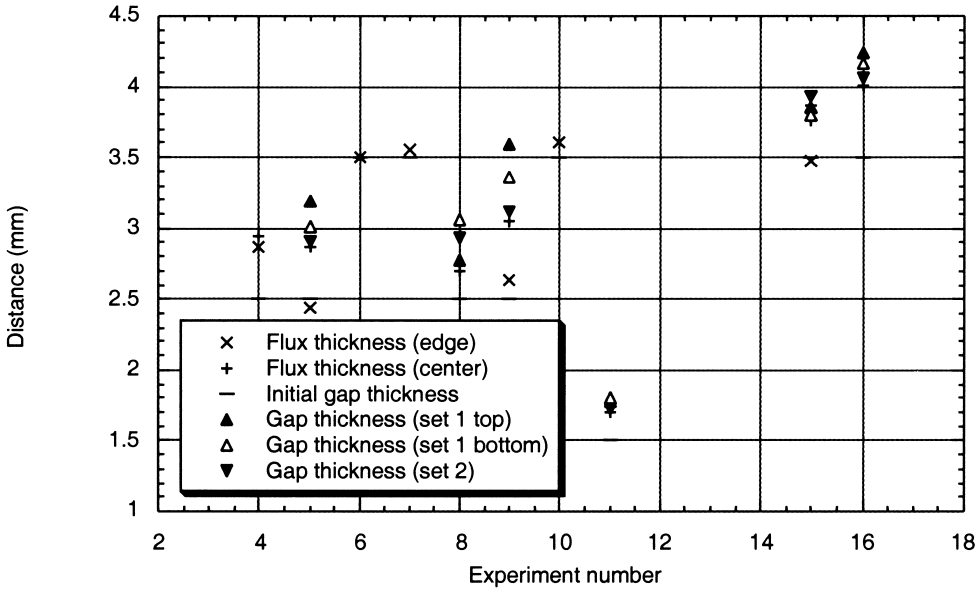

Fig. 9. Comparison of initial and final gap thicknesses with measured flux layer thickness.

These microstructures also reveal many voids that are believed to be gas bubbles that are evolved during solidification of the flux. These gas bubbles were clearly visible in every sample, except for the glassy flux A. This finding is consistent with the observations of Cramb and coworkers [2], who photographed such gas bubble formation during solidification of small samples of mold flux. Figure 11 shows that the bubbles sometimes form in just one of the layers, in this case the center. The drop in conductivity that should accompany these bands of gas voids is consistent with the observed low conductivity of the three crystalline fluxes.

PARAMETRIC STUDIES

The transient data collected for each experiment was divided into data points according to time periods, where conditions such as temperature remained constant for at least 100 s. Plots of conductivity and interface resistance were made for these data points in order to investigate the effects of gap thickness, temperature, and powder composition on the thermal properties.

Figure 13 shows the gap conductivity results, based on eqn (6). Figure 14 shows the flux conductivity predictions, based on eqn (7). There is a great deal of scatter in the results, and

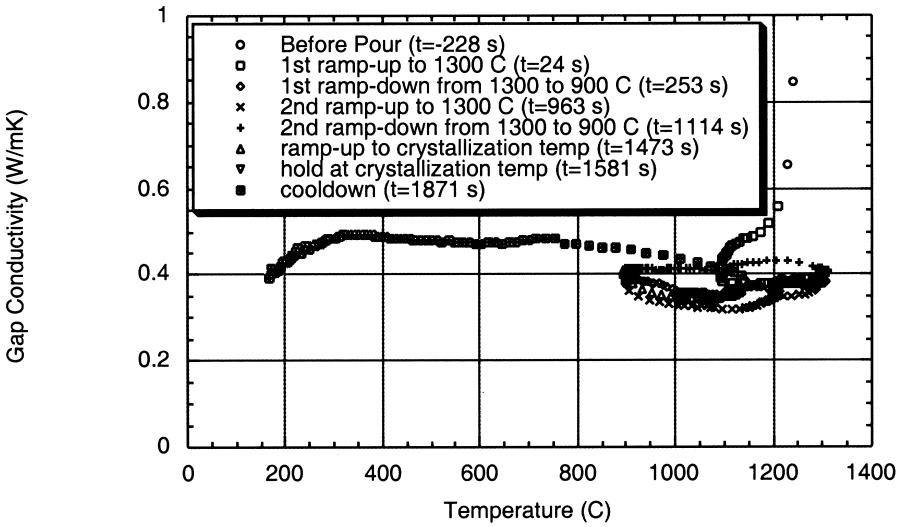

Fig. 10. Effective gap conductivity (experiment, set 1).

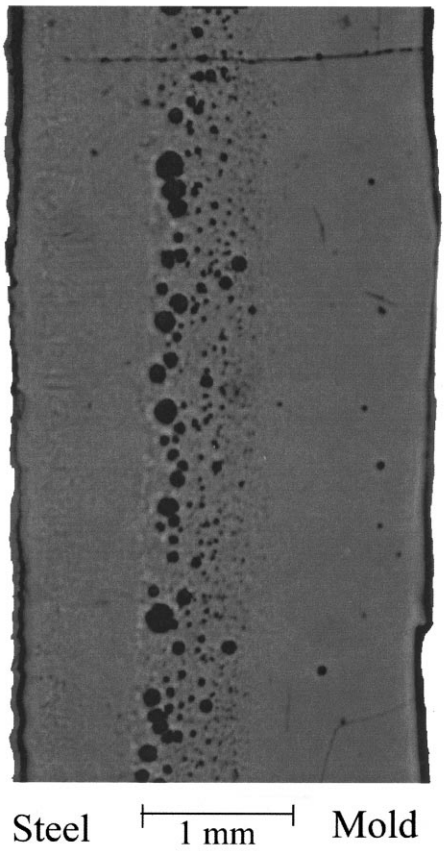

Fig. 11. Microstructure of section of solidified mold flux C (experiment 8, near edge).

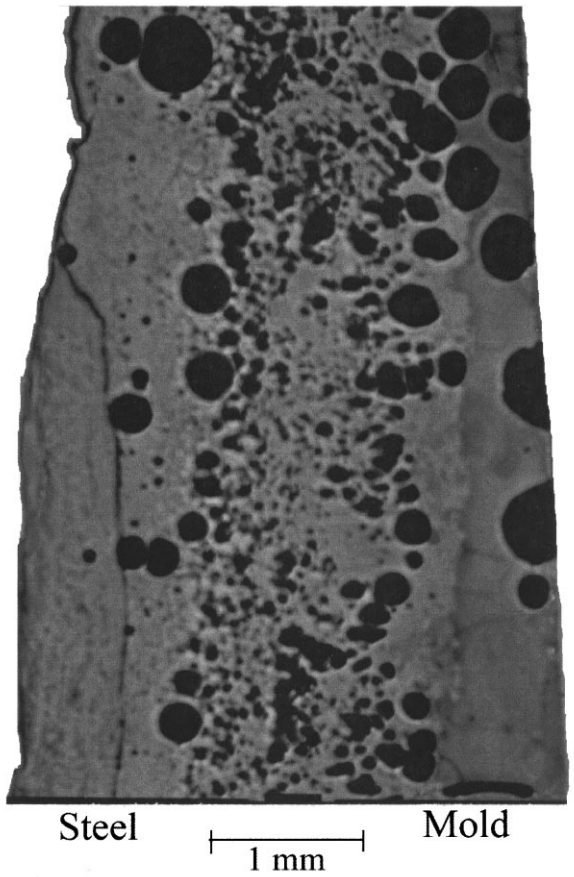

Fig. 12. Microstructure of section of solidified mold flux D (experiment 15, near thermocouple).

no significant trends can be seen for the effect of gap thickness or steel surface temperature on either of these conductivities. The gap conductivity ranges from 0.3–0.7 W/m·K (0.6 average). The flux conductivities are always higher and have more scatter, with a range of 0.5–2.0 W/m·K (1.0 average).

An interesting observation is that flux A had a much higher conductivity in one experiment (No. 2) (0.9 W/m·K gap conductivity). The observation of higher conductivity for flux A is consistent with its observed glassy structure, relative to the mainly crystalline structures of the other fluxes (B2, C, and D). This finding suggests that crystallinity is the only significant effect of flux composition on thermal properties, which agrees with the previous findings of Mills, discussed earlier.

Figures 15 and 16 show that the interface resistances also exhibit a great deal of scatter. They are also relatively insensitive to temperature, flux composition, and gap thickness. It is interesting that both interface resistances are equally large, ranging from 0–0.003 $m^2 \cdot K/W$. The flux/mold resistance sometimes showed negative values, which indicates both excellent contact and experimental error (variation). It was expected that the contact resistance should drop when the temperature increases above the flux melting temperature, especially at the flux/steel interface. This was not observed, which implies that the minor increase in plate warping at higher temperatures was more important.

MATHEMATICAL MODELS

The experimental results described in the previous section are being implemented into a 1-D transient heat flow—solidification model, called CON1D [16]. This model simulates temperature evolution in the mold, interface, and solidifying steel shell in the continuous casting mold. Details of the model are given elsewhere [16], but the important features of the interface model are repeated here. An improved interface model is needed in order to account for the complexities of the real continuous casting process that are not present in the simple experiment.

A more sophisticated model of heat flow across the gap is being applied, which augments the model in eqn (2) in several ways. Firstly, γ_1 is redefined to include the effects of interface resistances and oscillation marks:

$$\gamma_1 = \frac{1}{\left(\frac{d_a}{k_a} + \frac{d_s}{k_s} + \frac{d_l}{k_l} + \frac{d_{oeff}}{k_{oeff}}\right)} \tag{10}$$

Here, the interface resistances are lumped into a single term,

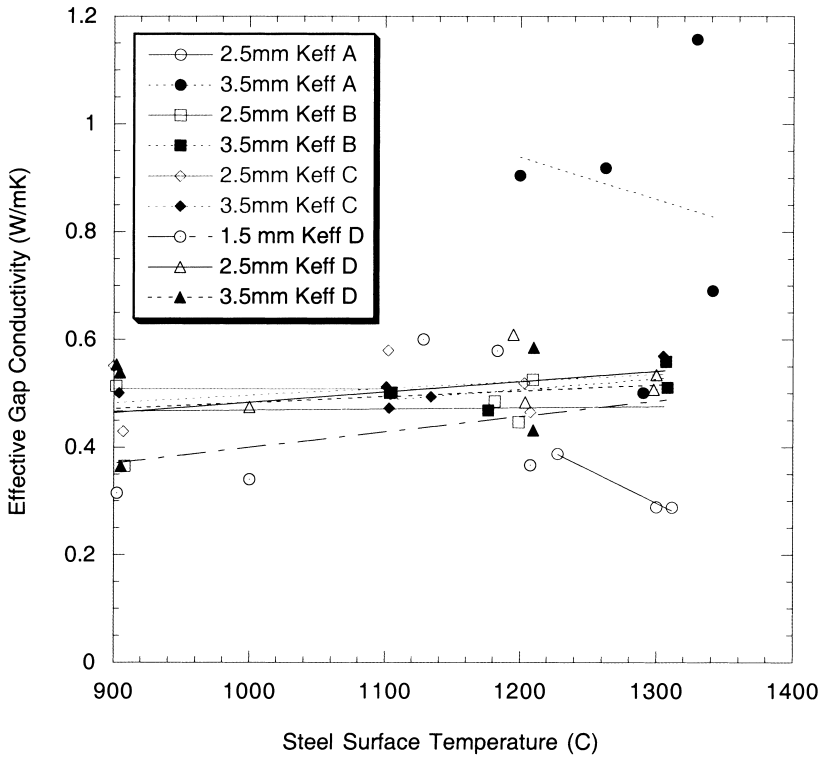

Fig. 13. Effective gap conductivity results.

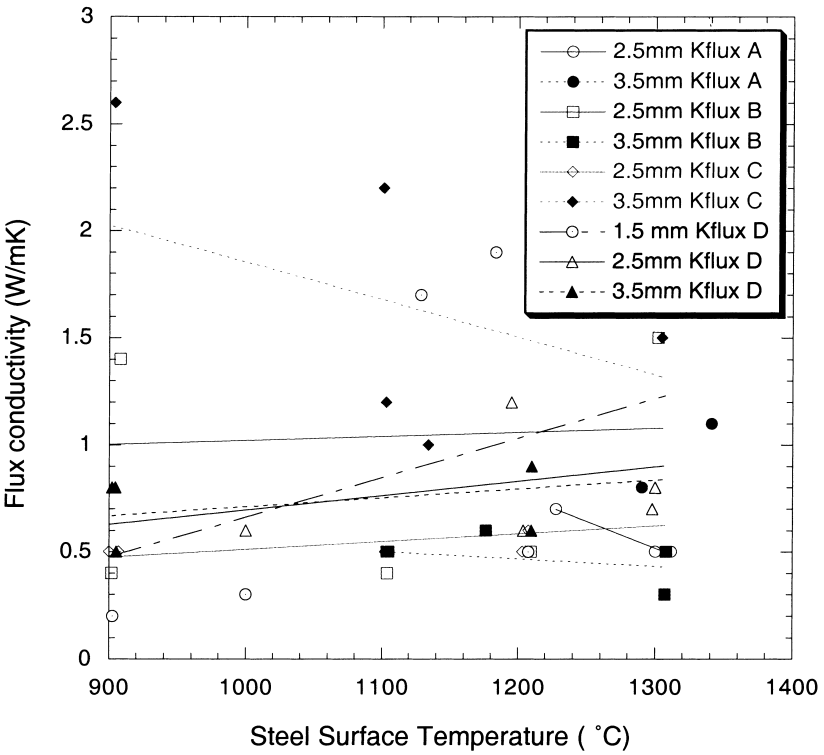

Fig. 14. Flux conductivity results.

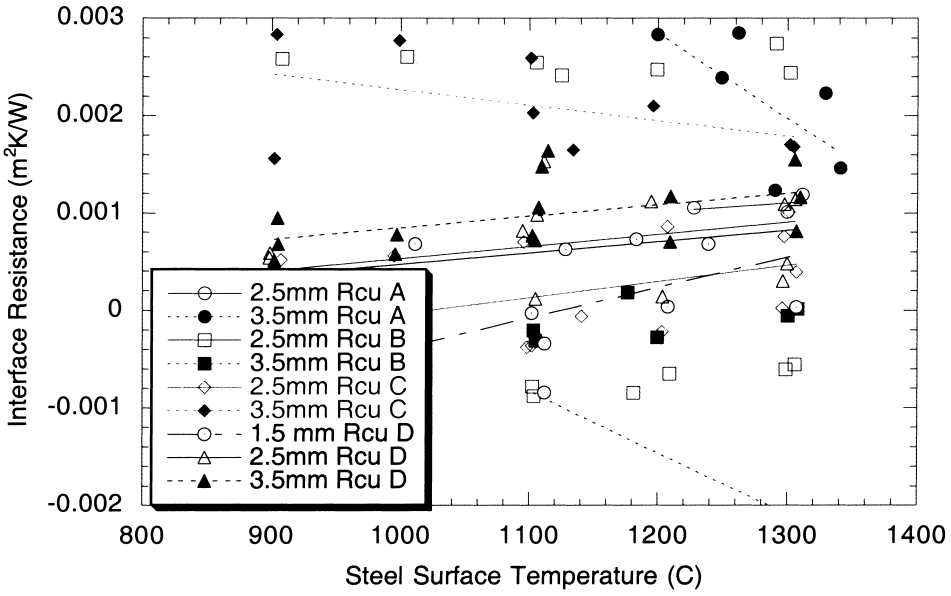

Fig. 15. Flux/mold interface resistance results.

which is expressed as an equivalent air gap size, d_a. Next, radiation is assumed to occur only while the flux is glassy, so structure and temperature data are used in evaluating the absorption coefficient in the second term in eqn (2).

The effective average thickness of the oscillation marks for heat transfer purposes, d_{oeff}, is calculated from:

$$d_{oeff} = \frac{0.5 L_{mark} d_{mark}}{(L_{pitch} - L_{mark})\left(1 + 0.5 \frac{d_{mark}}{(d_s + d_l)} \frac{k_f}{k_{mark}}\right) + L_{mark}} \quad (11)$$

The material filling the oscillation marks is assumed to be liquid mold flux, unless the steel surface temperature is

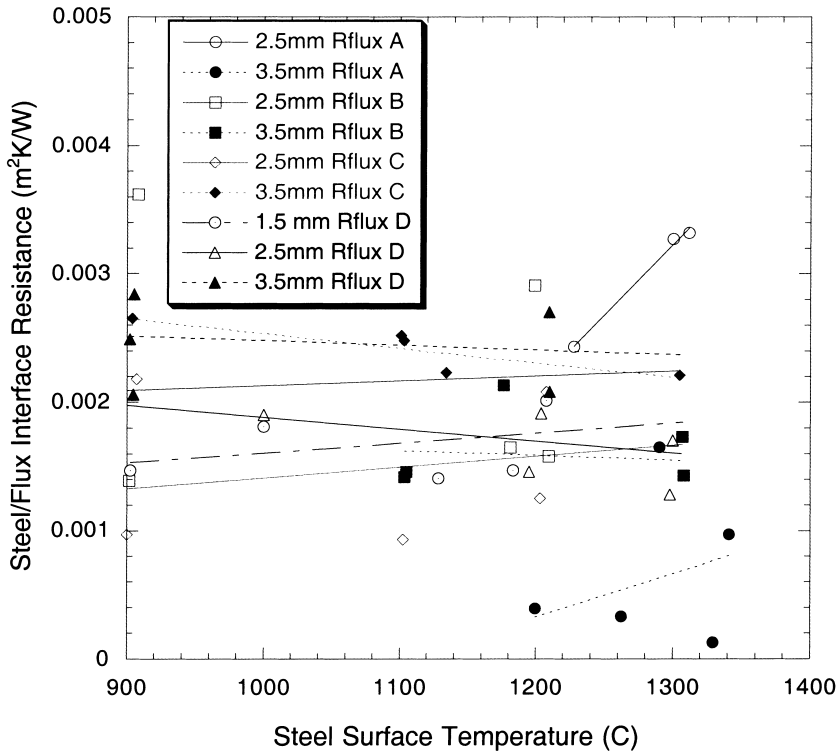

Fig. 16. Flux/steel interface resistance results.

below the glass transition or crystallization temperatures, or the consumption level is too small. In the latter cases, the oscillation marks become filled with air as needed.

Both mass and momentum balances are performed on the flux layers in the gap. Flux is assumed to flow down the gap as two distinct layers: solid and liquid. The solid layer is assumed to move at a uniform time-average velocity, V_s, which is always greater than or equal to zero and less than the casting speed, V_c, according to a time-dependent factor, f_s:

$$V_s = f_s V_c \tag{12}$$

This factor is found empirically during model calibration. The velocity profile in the liquid is found by solving a simplified Navier–Stokes equation that depends on the temperature-dependent viscosity of the flux [16].

A mass balance was imposed to express the fact that the known powder consumption, Q_f (kg m^{-2}), controls the total flow rate of casting flux past every location down the interfacial gap. Flux can be carried by the solid layer, liquid layer, or in the oscillation marks:

$$\frac{Q_f V_c}{\rho_{flux}} = V_s d_s + V_l d_l + V_c d_{osc} \tag{13}$$

The average depth of the oscillation marks (regarding their volume to carry flux), d_{osc}, is calculated from:

$$d_{osc} = \frac{0.5 L_{mark} d_{mark}}{L_{pitch}} \tag{14}$$

The model includes several other phenomena that are important to quantifying heat transfer in the continuous casting process. Examples include heat conduction through the mold to the water slots, solidification and cooling of the growing steel shell, and superheat delivery to the solidifying shell from the impinging liquid jet exiting the nozzle.

APPLICATIONS

The heat flow model presented in the previous section has many potential applications, once measured mold flux property data has been incorporated and it has been calibrated using industrial measurements. These applications include the prediction of: shell thickness at the mold exit to avoid breakouts; boiling in the cooling water channels; and the ideal narrow-face taper to match the shrinkage of the wide-face shell [17]. This is most useful for anticipating the behavior under different casting conditions. In addition, the temperatures calculated using CON1D can be input into a 2-D transient thermo-mechanical model, CON2D [18, 19], which simulates temperature, strain, distortion, stress, and crack damage in the solidifying shell. The CON1D model can also be applied to help investigate and understand the mechanisms of defect formation. Previous examples include investigations of surface depressions in continuous cast blooms [20], and low heat extraction problems with startup powders [21].

Finally, parametric studies can be performed to extract fundamental knowledge about the process. One such successful application of the model was to quantify the effect of oscillation marks on heat extraction and shell growth. This detailed study [22] revealed that most oscillation marks, at least on the wide face away from the corners, are filled with solidified mold flux (and not air). Deep (2 mm^2/cm) flux-filled oscillation marks drop shell growth by 6%. If these same oscillation marks were air filled, they would reduce shell growth by 20% and increase surface temperature by 300°C. This shows the important role that mold flux plays in making heat transfer in the mold more uniform. Many other interesting studies are possible with this model, once it has been calibrated using experimental and industrial data.

CONCLUSIONS

An experimental method has been developed and applied to measure the thermal properties of mold flux under conditions similar to those found in the meniscus region of a continuous casting machine. The experiment reproduces important aspects of the continuous casting process, including the temperature–time history experienced by the flux. Specific findings include:

1. The flux solidified in multiple layers similar to those observed from continuous casting molds and contained many gas bubbles.
2. Flux thermal properties may change with time. In particular, the flux conductivity appears to decrease with time.
3. The "measured" property values depend greatly on the model used to extract them. Flux conductivities in this work (including radiation but not interface resistances) averaged about 1.0 W/m·K.
4. Contact resistances at both interfaces were very important to heat transfer, especially in this particular apparatus, which simulates a rigid gap such as found in the corners of the continuous cast shell. Interface resistances averaged about 0.0015 m^2·K/W, which is equivalent to an air gap of about 0.1 mm.
5. Flux crystallization appears to be the only significant effect of flux composition. The one glassy flux tested had much greater thermal conductivities, presumably due to radiation transport.
6. Temperature and gap thickness had negligible effect on the properties.

More work is needed on both the experiments and their theoretical analysis. The results of this work are crucial for the accurate calibration of heat transfer models of the continuous casting process that include a reasonable treatment of the phenomena present in the gap. These models can then be applied to a wide range of practical issues.

Acknowledgements—The authors wish to thank Ron J. O'Malley and coworkers at the Armco Technology Center, Middletown, OH, for their extensive efforts to develop and help perform the experiments. This work was supported by the Continuous Casting Consortium at the University of Illinois (Allegheny Ludlum, Armco Inc., Columbus Stainless, LTV Steel, Ispat Inland Inc., and Stollberg Inc.), and the National Science Foundation (Grant DMI-98-00274) for which the authors are grateful.

REFERENCES

1. Jenkins, M. S. Characterisation and Modification of the Heat Transfer Performance of Mold Powders. In: Steelmaking Conference Proceedings, Iron and Steel Society, Warrendale, PA, 1995. 78. p. 669–677.
2. Kashiwaya, Y., Cicutti, C. and Cramb, A. W. Crystallization Behavior of Mold Slags. Steelmaking Conference Proceedings, Iron and Steel Society, Warrendale, PA, 1998. 81. p. 185–191.
3. Wolf, M. M., Mold Heat Transfer and Lubrication Control—Two Major Functions of Caster Productivity and Quality Assurance, In *Continuous Casting*, vol. 9, Iron and Steel Society, Warrendale, PA, 1997, pp. 211–229.
4. Emi, M. The Mechanisms for Sticking Type Breakouts and New Developments in Continuous Casting Mold Fluxes. Steelmaking Conference Proceedings, Iron and Steel Society, Warrendale, PA, 1991. 74. p. 639–646.
5. Susa, M., Mills, K. C., Richardson, M. J., Taylor, R. and Stewart, D., Thermal Properties of Slag Films Taken from Continuous Casting Mould, *Ironmaking and Steelmaking*, 1994, **21**(4), 279–286.
6. Stewart, D., Hewitt, P. N. and Peeters, L. The Prediction of Longitudinal Cracking During Slab Casting. Steelmaking Conference Proceedings, Iron and Steel Society, Warrendale, PA, 1996. 79. p. 207–214.
7. Kumar, S., Samarasekera, I. V. and Brimacombe, J. K., Mold Thermal Response and Formation of Defects in the Continuous Casting of Steel Billets. Part 2: Rhomboidity, *Iron and Steelmaker (ISS Transactions)*, 1998, **25**(12), 51–66.
8. Mikrovas, A. C., Argyropoulos, S. A. and Sommerville, I. D. Measurements of the Effective Thermal Conductivity of Liquid Slags and Mold Powders. Steelmaking Conference Proceedings, Iron and Steel Society, Warrendale, PA, 1990. 48. p. 103–112.
9. Mills, K. C., Olusanya, A., Brooks, R., Morrell, R. and Bagha, S., Physical Properties of Casting Powders. Part 4: Physical Properties Relevant to Fluid and Thermal Flow, *Ironmaking and Steelmaking*, 1988, **15**(5), 257–264.
10. Ohmiya, S., Tacke, K.-H. and Schwerdtfeger, K., Heat Transfer Through Layers of Casting Fluxes, *Ironmaking and Steelmaking*, 1983, **10**(1), 24–30.
11. Jenkins, M. S. Characterisation of Heat Transfer in a Continuous Casting Mold. Steelmaking Conference Proceedings, Iron and Steel Society, Warrendale, PA, 1995. 78. p. 315–320.
12. Taylor, R. and Mills, K. C., *Arch. Eissenhuttenwessen*, 1982, **53**, 55–63.
13. Susa, M., Li, F. and Nagata, K., Thermal Conductivity, Thermal Diffusivity, and Specific Heat of Slags Containing Iron Oxides, *Ironmaking and Steelmaking*, 1993, **20**(3), 201–206.
14. Mikrovas, A. C., Argyropoulos, S. A. and Sommerville, I. D., Heat Transfer Characteristics of Molten Slags, *Ironmaking and Steelmaking*, 1991, **18**(3), 169–181.
15. Yamauchi, A., Sorimachi, K., Sakuraya, T. and Fujii, T., Heat Transfer Between Mold and Strand Through Mold Flux Film in Continuous Casting of Steel, *ISIJ International*, 1993, **33**(1), 140–147.
16. Thomas, B. G., Ho, B. and Li, G., Heat Flow Model of the Continuous Slab Casting Mold, Interface, and Shell, In *Alex McLean Symposium Proceedings, Iron and Steel Society, Warrendale, PA*, 1998, pp. 177–193.
17. Lawson, G. D., Sander, S. C., Emling, W. H., Moitra, A. and Thomas, B. G. Prevention of Shell Thinning Breakouts Associated with Widening width Changes. Steelmaking Conference Proceedings, Iron and Steel Society, Warrendale, PA, 1994. 77. p. 329–336.
18. Moitra, A. and Thomas, B. G. Application of a Thermo-Mechanical Finite Element Model of Steel Shell Behavior in the Continuous Slab Casting Mold. Steelmaking Proceedings, Dallas, TX, 1993. 76. p. 657–667.
19. Moitra, A., *Thermo-mechanical Model of Steel Shell Behavior in Continuous Casting*. Ph.D. thesis, University of Illinois at Urbana-Champaign, 1993.
20. Jenkins, M. S., Thomas, B. G., Chen, W. C. and Mahapatra, R. B. Investigation of Strand Surface Defects using Mold Instrumentation and Modelling. Steelmaking Conference Proceedings, Iron and Steel Society, Warrendale, PA, 1994. 77. p. 337–345.
21. Jenkins, M. and Thomas, B. G. A Study of Mould Powder Related Start-up Problems. Steelmaking Conference Proceedings, Iron and Steel Society, Warrendale, PA, 1997. 80. p. 285–293.
22. Thomas, B. G., Lui, D. and Ho, B., Effect of Transverse and Oscillation Marks on Heat Transfer in the Continuous Casting Mold, In *Applications of Sensors in Materials Processing*, ed. V. Viswanathan, TMS, Warrendale, PA, Orlando, FL, 1997, pp. 117–142.